Coupled vegetation-precipitation variability observed from satellite and climate records

Alexander Lotsch, Mark A. Friedl, and Bruce T. Anderson
Department of Geography and Center for Remote Sensing, Boston University, Boston, Massachusetts, USA

Compton J. Tucker
Biospheric Sciences Branch, NASA Goddard Space Flight Center, Greenbelt, Maryland, USA

Received 8 April 2003; revised 16 May 2003; accepted 22 May 2003; published 30 July 2003.

[1] Variability in precipitation regimes at seasonal and longer time scales strongly influences ecosystem dynamics in arid and semi-arid regions. In this paper, we use time series of global precipitation and satellite normalized difference vegetation index (NDVI) data to analyze joint spatial and temporal variability between terrestrial ecosystems and precipitation regimes. Accumulated monthly rainfall anomalies are quantified using a standardized precipitation index (SPI), which provides a better measure of ecologically significant precipitation excess or deficit at growing season time scales relative to monthly precipitation data. Results from canonical correlation analysis reveal geographically extensive patterns of joint NDVI-SPI variability suggestive of strong climate-biosphere coupling. Further, leading modes of covariability are shown to be related to large-scale ocean-atmosphere circulation anomalies. These results illustrate the global extent and sensitivity of ecosystems susceptible to climate change-induced perturbations in precipitation regimes. *INDEX TERMS:* 0315 Biosphere/atmosphere interactions; 1854 Hydrology: Precipitation (3354); 1620 Global Change: Climate dynamics (3309); 1640 Global Change: Remote sensing. **Citation:** Lotsch, A., M. A. Friedl, B. T. Anderson, and C. J. Tucker, Coupled vegetation-precipitation variability observed from satellite and climate records, *Geophys. Res. Lett.*, *30*(14), 1774, doi:10.1029/2003GL017506, 2003.

1. Introduction

[2] Spatial and temporal patterns of biosphere-atmosphere interactions, including fluxes of carbon, water and energy, are intimately coupled to climate variability [*Bonan*, 2002], and substantial evidence suggests that important changes in these interactions will arise from projected climate change [*Clarke et al.*, 2001]. In particular, an enhanced global hydrologic cycle is expected to produce more extreme rainfall events and exacerbate naturally occurring droughts [*Trenberth*, 1998a]. In this context, geographic and seasonal patterns of vegetation-precipitation covariability has tremendous societal and ecological significance [*Stern and Easterling*, 1999].

[3] Precipitation is a primary control on vegetation dynamics in many tropical and subtropical biomes, including grasslands, savannas and forests. Climate induced disturbances in both the frequency and timing of precipitation result in observable ecosystem responses [*Knapp and Smith*, 2001] and also influence ecosystem productivity and terrestrial carbon sequestration [*Nemani et al.*, 2002]. In arid and semi-arid regions, soil moisture conditions provide a mechanism for sustained plant growth beyond individual rainfall events [*Nicholson et al.*, 1990]. While long-term average precipitation determines large-scale ecosystem and species distributions, variation in growing season precipitation can result in substantial inter- and intraannual variability in plant structure and productivity [*Woodward*, 1987].

[4] In recent years remote sensing observations have been used to examine the role of climate and climate anomalies in large-scale ecosystem dynamics. Specifically, the state and productivity of terrestrial ecosystems inferred from satellite-based observations have been linked to global atmospheric oscillation patterns [*Los et al.*, 2001], sea surface temperature (SST) anomalies [*Myneni et al.*, 1996; *Anyamba et al.*, 2002], decadal scale trends in CO_2 and temperatures [*Myneni et al.*, 1997], interannual temperature variability [*Braswell et al.*, 1997], and atmospheric cooling induced by aerosols [*Lucht et al.*, 2002].

[5] While plot scale studies reflect local ecohydrological conditions in vegetation-precipitation relations [*Knapp and Smith*, 2001], remote sensing provides a means to monitor geographically extensive patterns of coupled climate and vegetation processes. In particular, times series of National Oceanic and Atmospheric Administration (NOAA) Advanced Very High Resolution Radiometer (AVHRR) based vegetation inventories provide high temporal sampling and global geographic coverage suitable for studying large-scale vegetation dynamics [*Los et al.*, 2001]. The normalized difference vegetation index (NDVI) derived from red and near-infrared reflectances is proportional to the amount of absorbed photosynthetically active radiation [*Myneni et al.*, 1995] and is closely coupled to net primary productivity (NPP) and canopy structure [*Tucker and Sellers*, 1986]. In regions where precipitation is limited, NDVI data derived from satellites has been shown to be related to annually integrated precipitation [*Tucker and Nicholson*, 1999].

2. Data

[6] In this paper we use global 232-month (19.3 years) time series of precipitation and vegetation data to identify statistically significant dynamics in ecosystems that are related to seasonal and interannual variability in global precipitation regimes. For this analysis, global gridded time series of monthly NDVI derived from July 1981 to October 2000 NOAA-AVHRR data at 1 degree spatial resolution serve as a surrogate for vegetation activity. These data have been preprocessed to provide a spatially and temporally

Copyright 2003 by the American Geophysical Union.
0094-8276/03/2003GL017506$05.00

consistent representation of global vegetation for climate studies [*Tucker et al.*, 2003].

[7] Data from the Climate Prediction Center (CPC) Merged Analysis of Precipitation (CMAP) is used to quantify global patterns of ecologically significant water surplus and deficit. This data set provides mean global daily precipitation (mm/day) for each month from 1979 to 2001 at 2.5 degree spatial resolution. The CMAP data set is produced by merging gauge observations, precipitation estimates from five different satellite-based algorithms, and output from numerical model predictions [*Xie and Arkin*, 1997]. For this work, we converted the CMAP time series at each grid point to values of the standardized precipitation index (SPI) [*McKee et al.*, 1993]. The SPI is calculated from long-term precipitation records and provides a normalized and spatially invariant measure of relative precipitation anomalies at multiple time scales. The time scale is application-dependent and quantifies the accumulated precipitation anomaly over a specified time period leading up to and including the season of interest.

3. Analysis Techniques

[8] Prior to analyzing joint variability in NDVI and SPI the seasonal cycle was removed from both data sets ($\mu_{season} = 0$) and an exploratory analysis was performed to determine the appropriate time scale for computing the SPI. Figure 1 shows the average grid point correlation coefficients for NDVI and SPI time series calculated for major land cover classes at time scales of 1–12 months. These results show that ecosystems in arid and semi-arid climate regimes (shrublands, savannas, grasslands) are most sensitive to seasonal precipitation anomalies at time scales of 4–6 months, whereas forested land areas exhibit weak correlation with rainfall anomalies at all time scales. This observation is consistent with the concept of lagged vegetation response to soil moisture anomalies in arid and semi-arid climate regions [*Nicholson et al.*, 1990]. Thus, the 5-month SPI was used for subsequent analyses.

[9] To study the joint variability of SPI and NDVI we used linear canonical correlation analysis (CCA). CCA estimates pairs of time series, taken from two multivariate data sets, that are maximally correlated. The time series are estimated using an eigenvalue decomposition of the cross-covariance matrix of the two data sets [*Bretherton et al.*, 1992]. In this case, CCA computes linear combinations of monthly NDVI that are maximally correlated with linear combinations of SPI data. Specifically, since SPI reflects seasonally integrated precipitation, correlation between SPI and NDVI data are indicative of changes in vegetation induced by rainfall anomalies. The results from CCA include a set of canonical factors (CFs), which are time series sorted by descending correlation. To focus the analysis on the dominant modes of covariability we performed CCA using standardized, seasonal-mean and area-weighted leading principal components [*Barnett and Preisendorfer*, 1987]. The results presented were estimated from 78 seasonal means (i.e., 4 seasons per year) and were tested at a 5% significance level ($r \geq \pm.22$) using a two-tailed t-test.

4. Results and Discussion

[10] Monthly grid point correlation maps for 5-month SPI and NDVI are shown in Figure 2. This map identifies

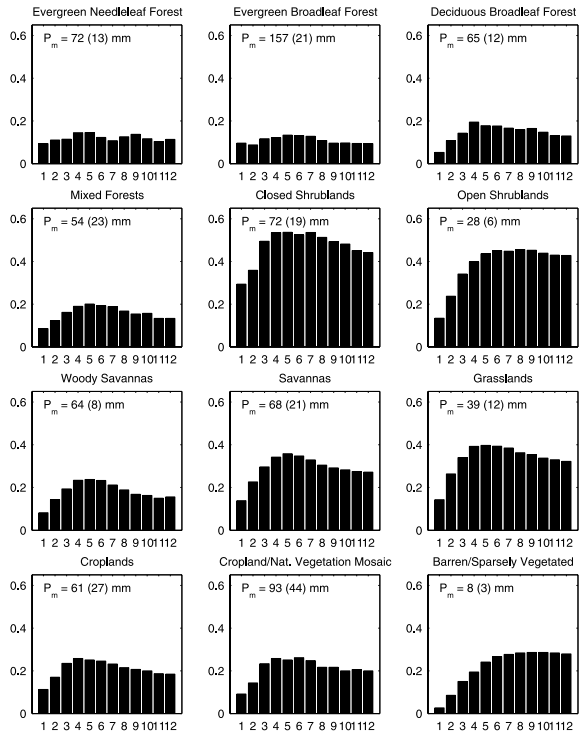

Figure 1. Distribution of average grid point correlation coefficients (y-axis) for 1–12 month SPI (x-axis) and NDVI for land cover classes defined by the International Geosphere Biosphere Programme. Monthly seasonal means show the highest correlations for shrublands, savannas and grasslands at growing season time scales (4–6 months). Average monthly precipitation totals P_m (mm) and standard deviations (in parenthesis) were calculated from 1979–2000 CMAP monthly precipitation records.

regions in which seasonally integrated precipitation anomalies correlate with NDVI anomalies and highlights arid and semi-arid climate regions. By using CCA, we are able to expand this result to isolate correlated modes of joint variability within the SPI and NDVI data sets. In particular, at continental to global scales CCA reveals geographically extensive patterns of joint NDVI-SPI variability that are clearly related to joint variation in ecosystem-climate dynamics.

[11] For brevity, only the leading modes (i.e., the modes explaining the most covariance) of seasonal canonical variability for North and South America, Africa and Australia are shown (no significant patterns were found for Eurasia). Figure 3 presents the CF time series (top) and corresponding correlation maps for NDVI (middle) and SPI (bottom). The eigenvalue, e, related to each mode is equivalent to the correlation coefficient between the transformed NDVI and SPI time series. The degree of association is strong for all four subsets ($0.69 \leq e \leq 0.79$) and the centers of action in each map are co-located, indicating precipitation-related NDVI anomalies.

[12] Comparison of the CCA results with circulation features (maps not shown) derived from the National Center for Environmental Prediction (NCEP) reanalysis [*Kalnay et al.*, 1996] reveal well defined physical mechanisms that explain the observed joint variation. Specifically, the lead-

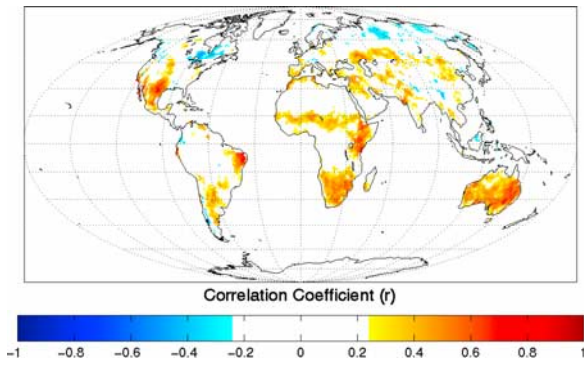

Figure 2. Significant grid point correlations ($r > .22$; $p = .05$) for monthly seasonal averages of 5-month SPI and NDVI. Positively correlated (red) areas suggest precipitation-vegetation coupling, whereas negatively correlated (blue) areas indicate snow or cloud cover effects.

ing mode for North America ($e = .69$) is characterized by opposing patterns of precipitation between the western U.S. and the southern great plains. Precipitation and NDVI anomalies in the south-west are spatially coincident and extend across northern central Mexico and southern parts of Texas and New Mexico (Figure 3A). In contrast, precipitation anomalies in the west (Sierra Nevada mountains and Upper Colorado River basin) are displaced with respect to the corresponding NDVI anomalies (southern Colorado River basin and parts of the Central Valley). This displacement reflects the response of irrigation patterns in southern California and Arizona to variability in precipitation regimes in the Sierra Nevada and Upper Colorado River Basin [*Gollehon and Quinby*, 2000]. Most of the variance in this SPI-NDVI pattern is associated with springtime NDVI-SPI variability. The SPI anomaly in this season, i.e. the integrated rainfall anomalies over the previous 5 months, are primarily related to rainfall anomalies in March–May (MAM) and November–January (NDJ). Both MAM and NDJ are associated with a large mid-latitude trough at 500mb height, extending from the Gulf of Alaska to the eastern US with a ridge to the south extending from Hawaii to central Mexico. In MAM, this ridge is associated with negative anomalies in 500mb vertical velocities over western Mexico, and possibly a late arrival of the monsoon rains to this region [*Yu and Wallace*, 2000]. In NDJ, the continental scale trough is related to a south-eastern shift of the subtropical jet stream over the Gulf of Mexico with anomalous negative vertical velocities to the west of the entrance region, resulting in decreased precipitation over central Mexico. Excess precipitation in the western part of the continent correlates with a southerly shift in the Pacific jet stream related to large-scale circulation features over the central/eastern tropical Pacific and the Gulf of Alaska [*Dettinger et al.*, 1998].

[13] Figure 3B shows South America's leading mode ($e = .75$), which has the highest variability in June–August (JJA) and is characterized by a typical El-Niño type response pattern with two dipoles centered in north-eastern Brazil and an area extending from southern Brazil to the Argentinian pampas [*Paegle and Mo*, 2002]. SPI anomalies in JJA arise from precipitation anomalies during the austral late summer and fall (February–May). The SPI-NDVI patterns correlate with 500mb vertical velocity anomalies over these two regions and are related to warm waters in the

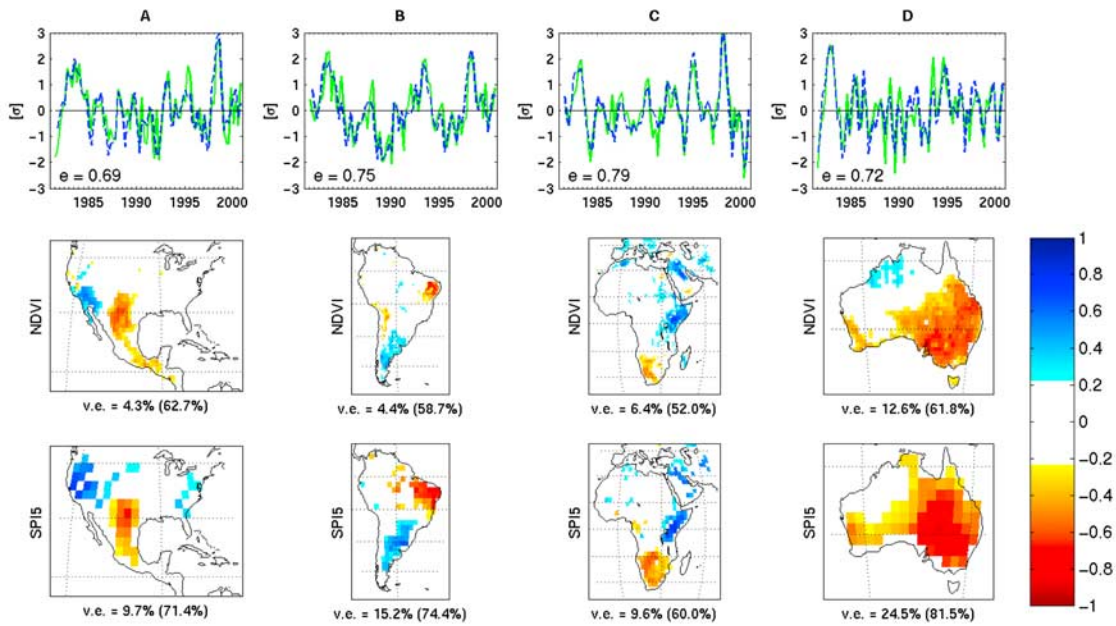

Figure 3. Leading canonical modes of joint SPI-NDVI variability for North America, South America, Africa and Australia identified by CCA. (top panels: NDVI - solid line, SPI - dashed line). Middle panels and bottom panels show correlation maps for NDVI and SPI, respectively. Only significant grid cells ($r >. 22$; $p =.05$) are shown. Each figure is labeled with the amount (percentage) of variance explained (v.e.) by each component and the total amount of variance included in the analysis (in parenthesis) using m leading principal components of NDVI and SPI ($m = 10$, except $m = 7$ for Australia).

eastern equatorial Pacific, along with cold Atlantic waters off the Brazilian coast.

[14] The leading mode for Africa ($e = .79$) is characterized by a dipole pattern with centers in southern Africa and the horn of Africa (Figure 3C). Also, the Arabian peninsula and parts of central Asia exhibit strong joint variability, with December–February (DJF) showing the strongest correlations. Positive summertime rainfall anomalies in southern Africa are related to a south-westerly shift of the subtropical high induced by La Niña conditions over the eastern equatorial Pacific (e.g., 1984/85, 1994/95), which displaces the summertime inter-tropical convergence zone (ITCZ) southward. Anomalies in the horn of Africa are associated with subsidence over the Indian ocean, extending over eastern Africa. These conditions are related to La Niña and cold SST anomalies over the Indian ocean [*Anyamba et al.*, 2002].

[15] The leading mode for Australia ($e = .72$) exhibits the most variability in the austral spring (September–November) and arises largely from precipitation anomalies in the previous winter (JJA), extending into spring (Figure 3D). Rainfall anomalies in this season are associated with a consistent pattern of tropospheric circulation anomalies over Australia and the south-west Pacific. Specifically, winters during the high index phase of the Southern Oscillation (SO) are characterized by low sea level pressure centered over Australia. This low pressure is associated with anomalies in 700mb meridional circulation over eastern Australia, which causes a weakening of the local winter Hadley circulation during positive SO events [*Drosdowsky and Williams*, 1991]. As a result, dry south-easterly flow over the northern part of the continent is weakened and moist intrusions of tropical air masses into eastern Australia are more frequent.

5. Conclusions

[16] In this paper we analyze the covariability of remotely sensed NDVI and assimilated precipitation records. The high degree of association between NDVI and 5-month SPI time series indicate that SPI data capture ecologically significant accumulated precipitation surplus or deficit. The primary modes of joint temporal and spatial variability of NDVI and SPI at continental scales indicate that interannual variability in ecosystem dynamics in water limited regions is tightly coupled to variability in precipitation regimes. Further, comparison of canonical modes of variability in NDVI and SPI with changes in both atmospheric dynamics and circulation patterns show that the atmosphere functions as a bridge that propagates oceanic and atmospheric anomalies across continental scales [*Trenberth et al.*, 1998b], with important impacts on large-scale terrestrial ecosystems. The degree of observed coupled behavior between NDVI and SPI suggests that terrestrial ecosystems may be quite sensitive to perturbations in global precipitation regimes induced by climate change.

[17] **Acknowledgments.** This research was funded by the NASA Intelligent Data Understanding Program, Grant # NCC2-1245.

References

Anyamba, A., et al., From El Niño to La Niña: Vegetation response patterns over east and southern Africa during the 1997–2000 period, *J. Climate*, *15*, 3096–3103, 2002.

Barnett, T. P., and R. Preisendorfer, Origins and levels of monthly and seasonal forecast skill for United States surface air temperatures determined by canonical correlation analysis, *Mon. Weather Rev.*, *115*, 1825–1850, 1987.

Bonan, G. B., *Ecological Climatology: Concepts and Applications*, Cambridge University Press, Cambridge, 2002.

Braswell, B. H., et al., The response of global terrestrial ecosystems to interannual temperature variability, *Science*, *278*, 870–872, 1997.

Bretherton, C. S., et al., An intercomparison of methods for finding coupled patterns in climate data, *J. Climate*, *5*, 541–560, 1992.

Clarke, G. K. C., et al., Physical climate processes and feedbacks, in *Climate Change 2001: The scientific basis*, edited by J. T. Houghton et al., Cambridge University Press, Cambridge, 2001.

Dettinger, M., et al., North-south precipitation patterns in western North America on interannual-to-decadal timescales, *J. Climate*, *11*, 3095–3111, 1998.

Drosdowsky, W., and M. Williams, The Southern Oscillation in the Australian Region. Part I: Anomalies at the extremes of the oscillation, *J. Climate*, *4*, 619–638, 1991.

Gollehon, N., and W. Quinby, Irrigation in the American west: Area, water and economic activity, *Int. J. Water Resour. D.*, *16*, 187–195, 2000.

Kalnay, E., et al., The NCEP/NCAR 40-year reanalysis project, *B. Am. Meteorol. Soc.*, *77*, 437–470, 1996.

Knapp, A. K., and M. D. Smith, Variation among biomes in temporal dynamics of aboveground primary production, *Science*, *291*, 481–484, 2001.

Los, S. O., et al., Global interannual variations in sea surface temperature and land surface vegetation, air temperature, and precipitation, *J. Climate*, *14*, 1535–1549, 2001.

Lucht, W., et al., Climatic control of the high-latitude vegetation greening trend and Pinatubo effect, *Science*, *296*, 1687–1689, 2002.

McKee, T. B., et al., The relationship of drought frequency and duration to time scales, In *Proc. 8th Conference on Applied Climatology*, January 17–22, 179–184, Am. Meteorol. Soc., Boston, MA, 1993.

Myneni, R. B., et al., The interpretation of spectral vegetation indexes, *IEEE Trans. Geosci. Remote Sens.*, *33*, 481–486, 1995.

Myneni, R. B., et al., Satellite-based identification of linked vegetation index and sea surface temperature anomaly areas from 1982–1990 for Africa, Australia and South America, *Geophys. Res. Lett.*, *23*, 729–732, 1996.

Myneni, R. B., et al., Increased plant growth in the northern high latitudes from 1981 to 1991, *Nature*, *386*, 698–702, 1997.

Nemani, R., et al., Recent trends in hydrologic balance have enhanced the terrestrial carbon sink in the United States, *Geophys. Res. Lett.*, *29*, 1061–1064, 2002.

Nicholson, S. E., et al., A comparison of the vegetation response to rainfall in the Sahel and east Africa using normalized difference vegetation index from NOAA AVHRR, *Climatic Change*, *17*, 209–241, 1990.

Paegle, J. N., and K. C. Mo, Linkages between summer rainfall variability over South America and sea surface temperature anomalies, *J. Climate*, *15*, 1389–1407, 2002.

Stern, P. C., and W. E. Easterling, *Making climate forecasts matter*, National Academy Press, Washington, 1999.

Trenberth, K. E., Atmospheric moisture residence times and cycling: Implications for rainfall rates and climate change, *Climatic Change*, *39*, 667–694, 1998a.

Trenberth, K. E., et al., Progress during TOGA in understanding and modeling global teleconnections associated with tropical sea surface temperatures, *J. Geophys. Res.*, *103*, 14,291–14,324, 1998b.

Tucker, C. J., et al., The Global Inventory Mapping and Monitoring Study 1981–2002 AVHRR 8-km Data Set, *Photogram. Eng. Remote Sens.*, in press, 2003.

Tucker, C. J., and S. E. Nicholson, Variation in the size of the Sahara Desert from 1980 to 1997, *Ambio*, *28*, 587–591, 1999.

Tucker, C. J., and P. J. Sellers, Satellite remote sensing of primary production, *Int. J. Remote Sens.*, *7*, 1395–1416, 1986.

Woodward, F. I., *Climate and plant distribution*, Cambridge University Press, London, 1987.

Xie, P., and P. A. Arkin, Global precipitation: A 17-year monthly analysis based on gauge observations, satellite estimates and numerical model outputs, *B. Am. Meteorol. Soc.*, *78*, 2539–2558, 1997.

Yu, B., and J. M. Wallace, The principal mode of interannual variability of the North American monsoon system, *J. Climate*, *13*, 2794–2800, 2000.

A. Lotsch, M. A. Friedl, and B. T. Anderson, Department of Geography and Center for Remote Sensing, Boston University, Boston, MA 02215, USA. (alotsch@bu.edu; friedl@bu.edu; brucea@bu.edu)

C. J. Tucker, Biospheric Sciences Branch, NASA Goddard Space Flight Center, Greenbelt, MD 20771, USA. (compton@ltpmailx.gsfc.nasa.gov)